Chemical Engineering & Processing: Process Intensification 169 (2021) 108632

Contents lists available at ScienceDirect

Chemical Engineering and Processing - Process Intensification

journal homepage: www.elsevier.com/locate/cep

Efficient adsorption of Basic Blue 41 from textile wastewaters by natural and magnetically modified Manisa-Gördes clinoptilolite

Gülşah Mersin [a,*], Ünsal Açıkel [b], Menderes Levent [c]

[a] Uşak University Technology Transfer Office, Project Support Unit, Rectorate Ground Floor, 64000, Uşak, Turkey
[b] Cumhuriyet University, Faculty of Engineering, Chemical Engineering Department, 58140, Sivas, Turkey
[c] Uşak University, Faculty of Engineering, Chemical Engineering Department, 64000, Uşak, Turkey

ARTICLE INFO

Keywords:
Basic Blue 41
Clinoptilolite
Zeolite
Magnetic zeolite
Adsorption
Isotherm

ABSTRACT

A new magnetic zeolite was prepared by the chemical co-precipitation of Fe^{2+} and Fe^{3+} in the presence of natural Manisa- Gördes clinoptilolite. The adsorption of Basic Blue 41 (BB41) from aqueous solutions on natural and magnetically modified zeolite were studied at 298–323 K in a batch system. Natural and magnetic zeolites were characterized by N_2adsorption-desorption, XRD, FTIR, SEM-EDX and VSM analyses. Compared to natural zeolite, S_{BET}-specific surface area of magnetic zeolite increased by modification process. XRD pattern and FTIR spectra of magnetic zeolite showed the characteristic Fe_3O_4 peaks. Optimum parameters were determined based on the experimental data by investigating the various parameters such as pH, initial dye concentration, adsorbent dosage, adsorbent particle size, contact time, stirring speed and temperature. Adsorption isotherms and kinetics were analyzed using Langmuir, Freundlich, Dubinin-Radushkevich (D-R), Temkin, Pseudo first order and Pseudo second order models. Adsorption of BB41 on natural and magnetic zeolites well fitted to Langmuir isotherm and pseudo second order kinetic models. The maximum adsorption capacities of natural and magnetic zeolites were determined as 149.25 mg/g and 370.37 mg/g at 323 K, respectively. Thermodynamic analysis revealed a spontaneous and endothermic nature of natural and magnetic zeolites.

1. Introduction

Nearly 50% of the dyes used in the textile industry are not fixed to surface of the textile fiber due to the lack of affinity and can be toxic in wastewaters even at small concentrations [1]. Textile wastewaters are characterized with high in color and salinity due to alkaline dyes which are often used in the industry. Their complex structure and synthetic origin in water make them difficult to remove. Biological, chemical, or physical methods are used for the treatment of textile wastewaters [2]. Among these techniques, adsorption is often preferred for the removal of dyes and other contaminants because of economical and simple [3]. Various adsorbents such as coconut fiber [4], phosphoric acid activated *Persea americana* nuts [5], boron-enriched nano clay [6], activated carbon prepared from filament algae [7] have been reported for the removal of BB41 from aqueous solutions. One of these adsorbents, natural zeolites are aluminosilicates commonly known as "molecular sieves" with three-dimensional space systems formed by uniform micropores [8]. Owing to these properties, crystal violet, congo red, safranin, methylene blue, can be effectively removed from aqueous solutions with cheap adsorbents such as zeolite-montmorillonite [9], zeolite-based polymer composites [10], heulandite, clinoptilolite, phillipsite [11] and kaolin [12]. The dye removal efficiency of zeolites can be increased with various surface modifications. Magnetic modification may enable the simple and efficient separation of adsorbents after the process with an external magnetic field [13]. In recent studies, magnetic zeolites have been successfully used for water treatment. Badeenezhad et al. (2019) investigated methylene blue adsorption in a batch mode with natural and magnetic clinoptilolite. Using natural zeolite, the removal efficiency of methylene blue found as 48% at pH: 9 [14]. Afshin et al. (2020) investigated the adsorption of cationic blue 41 with Zeolite/Fe_3O_4 nanocomposite. The kinetic data obeyed pseudo second order model whereas isotherm data fitted well by Freundlich isotherm model. 71.4% dye removal was achieved under optimum conditions [13]. Bayat et al. (2018) investigated methylene blue adsorption with clinoptilolite/nickel ferrite/sodium alginate nanocomposites which was synthesized by the co-precipitation method. The maximum adsorption capacity of methylene blue was determined as 54.05 mg/g [15]. Chang et al. (2016) investigated methylene blue adsorption with Fe_3O_4 activated

* Corresponding author: Uşak University Technology Transfer Office, Project Support Unit, Rectorate Ground Floor, 64000, Uşak, Turkey.
E-mail address: gulsah.mersin@usak.edu.tr (G. Mersin).

https://doi.org/10.1016/j.cep.2021.108632
Received 27 May 2021; Received in revised form 2 September 2021; Accepted 4 September 2021
Available online 10 September 2021

montmorillonite (Mt), (Fe_3O_4/Mt), nanocomposite. The removal efficiency was found as 99.47% of methylene blue in medium containing 100 mg/L initial concentration using 0.5 g Fe_3O_4/Mt. Adsorption kinetics and isotherms fitted well with the pseudo-second order and Langmuir models, respectively [16]. Nyankson et al. (2019) studied methylene blue adsorption with zeolite and zeolite-Fe_3O_4 nanocomposites. Experimental data showed that the adsorption kinetics fitted well to pseudo-second-order model. The maximum adsorption capacity was stated as 2.57 mg/g at 25 °C [17].

In the present study, the adsorption of BB41 dye from wastewater with natural and magnetically modified clinoptilolites was investigated in a laboratory scale. The characterization results and maximum adsorption capacity of magnetic zeolite have shown that it can be used as a new, alternative, and inexpensive adsorbent in wastewater treatment.

1.1. Mathematical description of the adsorption system

1.1.1. Adsorption isotherms

Adsorption isotherms provide important information to describe single-layer or multi-layer adsorption of BB41 on zeolite and magnetic zeolite. The amount of BB41 adsorbed per gram of zeolite and the adsorption efficiency were determined according to Eqs. (1) and (2) [18].

$$q_{e=\ \frac{(C_o-C_e)V}{m}} \tag{1}$$

$$Adsorption\ efficiency\% = \frac{C_o - C_e}{C_o} x100 \tag{2}$$

Where q_e is amount of dye adsorbed per gram of adsorbent at equilibrium (mg/g), C_o is initial dye concentration (mg/L), C_e is dye concentration at equilibrium (mg/L), m is weight of adsorbent, V is volume of dye solution (L). Equilibrium adsorption isotherm data were analyzed using Langmuir, Freundlich, Dubinin–Radushkevich (D-R), and Temkin isotherms. The Langmuir model describes monolayer and uniform sorption on distinct sites which means the active site adsorbed only one adsorbate molecule. The Langmuir equation can be written in the following linear form [16].

$$\frac{C_e}{q_e} = \frac{1}{q_m b} + \frac{1}{q_m} C_e \tag{3}$$

$$\frac{1}{q_e} = \frac{1}{q_m} + \frac{1}{b.q_m}\frac{1}{C_e} \tag{4}$$

The dimensionless separation factor R_L which describes the nature, and the feasibility of the adsorption process is represented as:

$$R_L = \frac{1}{1 + bC_0} \tag{5}$$

Where q_e is amount of dye adsorbed per gram of adsorbent at equilibrium (mg/g), q_m is maximum adsorption capacity (mg/g), C_o is initial dye concentration (mg/L), C_e is dye concentration at equilibrium (mg/L), b is Langmuir isotherm constant (L/mg). Isotherm type can be classified according to the R_L value. $R_L > 1$ is unfavorable, $R_L = 1$ linear isotherm, $0 < R_L < 1$ favorable isotherm, $R_L = 0$ is irreversible isotherm [15].

Freundlich isotherm is applicable to adsorption processes that occur on heterogenous surfaces. The linear form of the Freundlich isotherm is as follows:

$$lnq_e = lnK_F + \frac{1}{n} lnC_e \tag{6}$$

Where q_e is amount of dye adsorbed per gram of adsorbent at equilibrium (mg/g), q_m is maximum adsorption capacity (mg/g), K_F is Freundlich isotherm constant ((mg/g)(mg/L)$^{1/n}$), n is adsorption intensity. According to Eq. (6), the plot of lnC_e against Inq_e gives the slope and intercept as n and K_F respectively [19].

The Dubinin-Radushkevich (D-R) isotherm [20] model is a fundamental equation that describes the adsorption process occurred onto homogeneous and heterogeneous surfaces. Dubinin-Radushkevich isotherm model can be expressed using the following equation.

$$Inq_e = Inq_m - k_D\varepsilon^2 \tag{7}$$

$$\varepsilon = RTln(1 + 1/C_e) \tag{8}$$

Where q_e is amount of dye adsorbed per gram of adsorbent at equilibrium (mg/g), q_m is maximum adsorption capacity (mg/g), k_D is Dubinin-Radushkevich (D-R) isotherm constant (mol^2/kJ^2) (related to average free energy of adsorption per mole of adsorbate), ε is the Polanyi potential, R is universal gas constant (8.314×10^{-3} kJ/(molK)), T is temperature (K), E represents the sorption energy (kJ/mol). The plot of lnq_e against ε^2 yields a straight line. k_D and q_m values were obtained from slope and intercept, respectively. The sorption energy represented as E (kJ/mol) can be expressed by Eq. (9) as mentioned below.

$$E = (2k_D)^{\frac{1}{2}} \tag{9}$$

If the E value is in the 8–16 kJ/mol range, the adsorption is governed by ion exchange whereas less than 8 kJ/mol, by physical interactions. If the energy value is greater than 16 kJ/mol, the adsorption mechanism occurs by chemical interactions [21].

Temkin isotherm model assumed that the heat of adsorption of all molecules in the layer decreases linearly because of increased surface coating [22]. Temkin isotherm model is expressed as:

$$q_e = \frac{RT}{b_T} In(AC_e) \tag{10}$$

The linear form of Eq. (10) can be expressed as follow:

$$q_e = \frac{RT}{b_T} InA + \frac{RT}{b_T} InC_e \tag{11}$$

Eq. (12) obtained if B (RT/b_T B) is written instead of RT/b_T;

$$q_e = BInA + BInC_e \tag{12}$$

Where q_e is amount of dye adsorbed per gram of adsorbent at equilibrium (mg/g), q_m is maximum adsorption capacity (mg/g), A is equilibrium constant (L/g), b_T is Temkin isotherm constant (J/mol), R is universal gas constant (8.314×10^{-3} kJ/(molK)), T is temperature (K). A plot of q_e against InC_e yields a straight line with b_T and A determined using the slope and intercept, respectively [22].

1.1.2. Adsorption kinetics

Pseudo first order (PFO) and Pseudo second order (PSO) model fitting was carried out to understand either physical or chemical nature of dye-adsorbent interaction. The Lagergren pseudo first order kinetic model can be illustrated as Eqs. (13):

$$q_t = q_e\ (1 - exp(k_1 t)) \tag{13}$$

$$In(q_e - q_t) = Inq_e - k_1 t \tag{14}$$

Where q_e is amount of dye adsorbed per gram of adsorbent at equilibrium (mg/g), q_t is dye adsorbed at time t (mg/g), k_1 is the pseudo-first-order rate constant (min^{-1}), t is time (min). k_1 and q_e can be determined using the linear plot of t against In(q_e-q_t) [23]. If adsorption rate has a quadratic mechanism, the pseudo second order (PSO) model can be written as [19]:

$$\frac{dq_t}{dt} = k_2(q_e - q_t)^2 \tag{15}$$

$$\frac{t}{q_t} = \frac{1}{k_2 q_e^2} + \frac{1}{q_e} t \tag{16}$$

Where q_e is amount of dye adsorbed per gram of adsorbent at

equilibrium (mg/g), q_t is dye adsorbed at time t (mg/g), k_2 is the pseudo-second-order rate constant (g/(mgmin)), t is time (min). The value of q_e and k_2 was obtained from the slope and intercept of the linear plot of t vs t/q_t. According to the pseudo second kinetic model, the initial adsorption rate, h (mg/(gmin)) is expressed as follow:

$$h = k_2 q_e^2 \tag{17}$$

1.1.3. Adsorption thermodynamics

Adsorption thermodynamics give the information about the effect of temperature change on the adsorption mechanism. Thermodynamic parameters were determined using equations as below [20,23]:

$$\Delta G = \Delta H - T\Delta S \tag{18}$$

$$\Delta G = -RTInK_c \tag{19}$$

$$K_c = \frac{q_e}{C_e} \tag{20}$$

Where, ΔG is Gibbs free energy change (kJ/mol), ΔH is enthalpy change (kJ/mol), ΔS is entropy change (kJ/(mol K)), T is temperature (K), R is universal gas constant, q_e is amount of dye adsorbed per gram of adsorbent at equilibrium (mg/g), C_e is dye concentration at equilibrium (mg/L) and K_c is the equilibrium constant (L/mg).

By rearranging the Eqs. (18) and (19):

$$InK_c = \frac{\Delta S}{R} - \frac{\Delta H}{RT} \tag{21}$$

The values of ΔH/R and ΔS/R were determined from the slope and intercept of the Van't Hoff plot of $\ln K_c$ versus 1/T [21].

2. Material and method

2.1. Material

In present study, BB41 (Fig. 1) were provided by Kuyucak Textile in Uşak/Turkey. Natural zeolite, clinoptilolite ($(Na_{0.5}K_{2.5})(Ca_{1.0}Mg_{0.5})(Al_6Si_{30})O_{72}\bullet 24H_2O$), obtained from Gordes Zeolite Company in İzmir/Turkey. $FeSO_47H_2O$ (purity ≥ 99.0%) and NaOH (pure pellets), $FeCl_36H_2O$ (pure pellets ≥ 99.0%), NH_4OH (BioUltra, ~1 M NH_3 in H_2O) were purchased from Merck, Boston USA Chemistry, Sigma-Aldrich, respectively.

2.2. Preparation of BB41 stock solution

BB41 were used without any pretreatment. Stock solution was prepared by dissolving 1 g of BB41 in 1 L of distilled water. The test solutions were prepared by diluting of stock solution to the desired concentrations. The concentrations of solution varied in the range 20–200 mg/L. The pH of the solutions was adjusted with 0.1 N HNO_3 (purity ≥ 65.0%) and 0.1 N NaOH.

2.3. Preparation of unmodified natural clinoptilolite

Samples included particle size range of 0 −50 μ, 0 −200 μ and 0- 600 were washed with distilled water three times and separated using Whatman filter paper for the prediction of optimum value of particle size. After filtration, samples were dried in oven at 105 °C for 24 h. Although there was an overlap of the particle size in the range of 0–50, 50–200, 200–600 μ, a limitation in overlaps was not applied and adsorption of BB41 on natural and magnetic zeolites were investigated in a wider range. Such a limitation in particle size might be eliminated the effect of the particles on adsorption outside of the limitations.

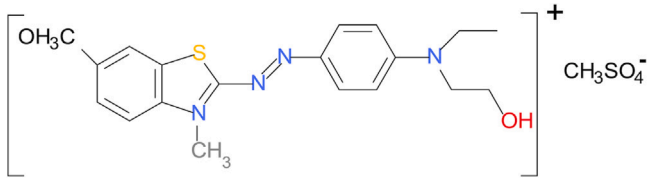

Fig. 1. Molecular structure of BB41 [21].

2.4. Synthesis of magnetically modified clinoptilolite

Magnetic zeolites were synthesized by the co-precipitation method. Two methods were chosen for prediction of zeolite/Fe and Fe^{2+}/Fe^{3+} weight ratio. The amount of zeolite and iron were adjusted to obtain the zeolite/iron oxide weight ratio of 3:1 [24] and Fe^{+2}/Fe^{+3} weight ratio 1:2 [25]. For the new synthesis method, 1 g of $FeSO_4\bullet 7H_2O$ and 2 g of $FeCl_3\bullet 6H_2O$ were dissolved in 100 mL of distilled water. Then, stirred at 450 rpm until the temperature reached 80 °C. When the temperature reached 80 °C, 40 mL of 25% NH_4OH solution was added and continued stirring until solution color alteration to black from yellow. When achieved black color, 8 g zeolite was added to the solution and 20 min was allowed for the reaction to complete. The solution was cooled at room temperature and the magnet was placed under the beaker. NH_4OH solution carefully was removed with a syringe and solution washed distilled water several times. Magnetic zeolite was separated by neodymium magnets and were dried at 75 °C for 30 h. This process was repeated for each particle size (0–50 μ, 0–200 μ, 0–600 μ) and it was seen that the method is reproducible. Chemical reactions that occur in the production of magnetic zeolites were shown as below:

$$FeSO_47H_2O + 2FeCl_36H_2O + 8NH_4OH \rightarrow Fe_3O_4 + 6NH_4Cl + (NH_4)_2SO_4 + 23H_2O \tag{22}$$

$$Fe_3O_4 + Z + 23H_2O \rightarrow Z\text{-}Fe_3O_4 \text{ (Magnetic zeolite)} \tag{23}$$

2.5. Physicochemical characterization of natural and magnetic zeolites

Natural and magnetic zeolites were characterized by XRD, SEM, EDX, BET, FTIR and VSM analysis. The characterization of zeolite and magnetic zeolite was made using the following equipment: The X-Ray Diffraction pattern was recorded in the scanning mode on a PAN analytical Empyrean analytical instrument operated at 4 kW (max 60 kV, max 100 mA). The structural morphology and Empirical elemental compositions of natural and magnetic zeolites were estimated using energy dispersive EDX-Zeiss Sigma 300 SEM equipment operated with 20 kV. The surface area and porosity measurement were determined using N_2-adsorption-desorption measurements on a Micromeritics Tristar model instrument under vacuum for 10 h at room temperature. Adsorbed gas volume was taken from the adsorption-desorption isotherm at p/p^0: 0.1–1.0. FTIR analysis was employed with a single bounce diamond anvil ATR accessory fitted to a Bruker VERTEX 70v FTIR spectrometer. The spectra were measured in the wave number range of 400–4000 cm^{-1}. Magnetic properties of synthesized zeolite were determined using Vibrating Sample Magnetometer (VSM)-LAKESHORE.

2.6. Batch adsorption experiments

Batch adsorption studies were investigated in the BB41 concentration range of 20–200 mg/L at 298–323 K. The pH of the solution was adjusted by adding diluted HNO_3 and NaOH. Batch equilibrium adsorption experiments were carried out by shaking 100 mL solution of various dye concentrations at pH 6.0, and 7.0 with 0.1 g natural and magnetic zeolites, respectively. All the adsorption experiments were conducted at 240 min and a stirring speed of 250 rpm in 250 mL beaker. 5 mL samples were centrifuged at 3000 x g for 7 min. and the supernatant fluid were analyzed for BB41 concentration. Adsorption of the

BB41onto natural and magnetic zeolites were monitored using UV–vis spectroscopy. 100 mg/L BB41 sample was scanned between 400 and 800 nm wavelengths in a Perkin Elmer Lambda 365 UV–vis spectrometer. The maximum wavelength of BB41 were observed at 610 nm [18].

3. Results and discussion

3.1. Physicochemical properties of natural zeolite and magnetic zeolite

3.1.1. N_2 adsorption-desorption analysis

N_2 adsorption-desorption isotherms of natural and magnetic zeolite provide information about the zeolite's structures at 77 K. It can be expressed using various methods, namely BET, BJH, t-plot and DFT. According to the results of N_2 adsorption-desorption characterization, specific surface area of magnetic zeolite was found larger than natural zeolite by BET, D-H, t-plot, and BJH methods due to coating zeolite surface with Fe_3O_4 nanoparticles (Fig. 2).

Langmuir surface areas of natural zeolite (Z) and magnetic zeolite (MZ) were determined as 274.54 m^2/g and 464.08 m^2/g respectively. Experimental data which was calculated from Langmuir isotherm confirmed these results with increased the adsorption capacity of magnetic zeolite. BET surface areas of natural zeolite (Z) and magnetic zeolite (MZ) were determined as 19.60 m^2/g and 25.57 m^2/g respectively [26]. It was clearly seen that surface modification with Fe_3O_4 particles can improve the surface area of natural zeolite. Nitrogen isotherms of zeolite and magnetic zeolite in Fig. 2 largely conformed to a type IV adsorption isotherm with type H3 hysteresis loop which was in the mesopores at p/p^0: 0.1–1.0 (d: 2–50 nm) [27]. In Fig. 2a and Fig. 2b, it was seen that there were considerable differences between the adsorption and desorption isotherms. The pressure range of these differences ($0.1 < p/p^0 < 0.3$) is particularly interesting as these differences also extend below the pressures ($p/p^0 > 0.3$) (Fig. 2b) was observed. In Fig. 2, pore filling occurred at higher relative pressures ($p/p^0 > 0.3$) and adsorbed gas volume decreased. The adsorbed gas volume by magnetic zeolite was higher than natural zeolite due to the increased pore volume of magnetic zeolite in Fig. 2b. The curve starting at p/p^0: 0.1–0.2 for magnetic zeolite showed that desorption started rapidly. But desorbed gas volume was found lower than natural zeolite at p/p^0: 0.1–1.0. It can be also observed with close adsorption and desorption curves of magnetic zeolite [28].

3.1.2. XRD analysis

Crystal phase and structural properties of the natural and magnetic zeolite were examined with XRD analysis which was carried out at room temperature and 2 h. Spectra were shown for the range of 2θ:0°–100°. The XRD patterns of the natural and magnetic zeolite were presented in Fig. 3. According to XRD data, natural zeolite (Z) was identified by its characteristic X-ray diffraction peaks at 2Θ:9.86°–11.14°–13.09°–17.26°–17.37°–20.91°–22.43°–26.64°–30.00°–30.18°–35.70°-36.96°- 39.45° as were reported in previous studies [29]. The unlabeled small peaks were unidentified impurities in natural zeolite. But it was clearly seen that the natural zeolite (Z) mainly consists of clinoptilolite. It was possible to see the high crystallinity of clinoptilolite with condensed peaks at 2Θ:9.92°–22.43°–30.50° [14,30]. It was reported that Manisa-Gördes zeolite was composed of a small amount of biotite, quartz, feldspar, and rock fragments and contains at least 90% clinoptilolite [31]. Current results of natural zeolite were similar to the findings of previous studies [32,33]. XRD pattern of the magnetic zeolite were shown in Fig. 3. The characteristic peaks located at 2Θ:8.86°-9.96°–11.14°–13.27°–14.85°–17.23°–20.83°–22.41°–26.11°–29.97°–31.91°–37.04°–43.94°–57.81°–62.25° matched with standard diffraction peaks of Fe_3O_4 [13]. Fig. 3 shows that the characteristic dispersion peaks of magnetic zeolite at 2θ:30.28°–35.70°–57.81° were significantly strengthened after magnetic modification which were similar to the previous reports [17,34]. In Fig. 3, a slight decrease was observed in the density of diffraction peaks of magnetic zeolite. Magnetization with iron ions led to a decrease in crystallinity and an increase in porosity. It might be resulted from the partial removal of the exchangeable cations on structure of the natural zeolite [35]. Sharp peaks and negligible changes after magnetic modification indicated that the adsorbents possess a high degree of crystallinity and structural

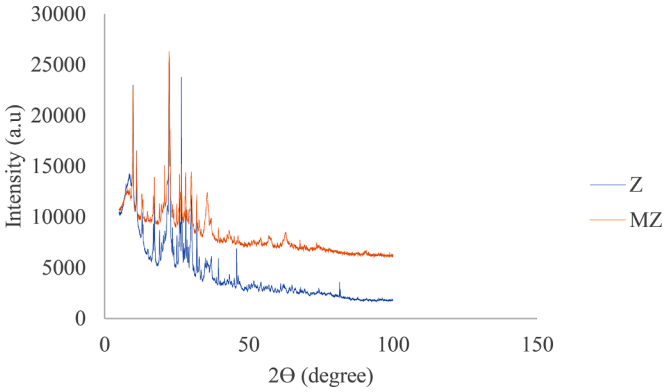

Fig. 3. XRD analyses of natural zeolite (Z) and magnetic zeolite (MZ).

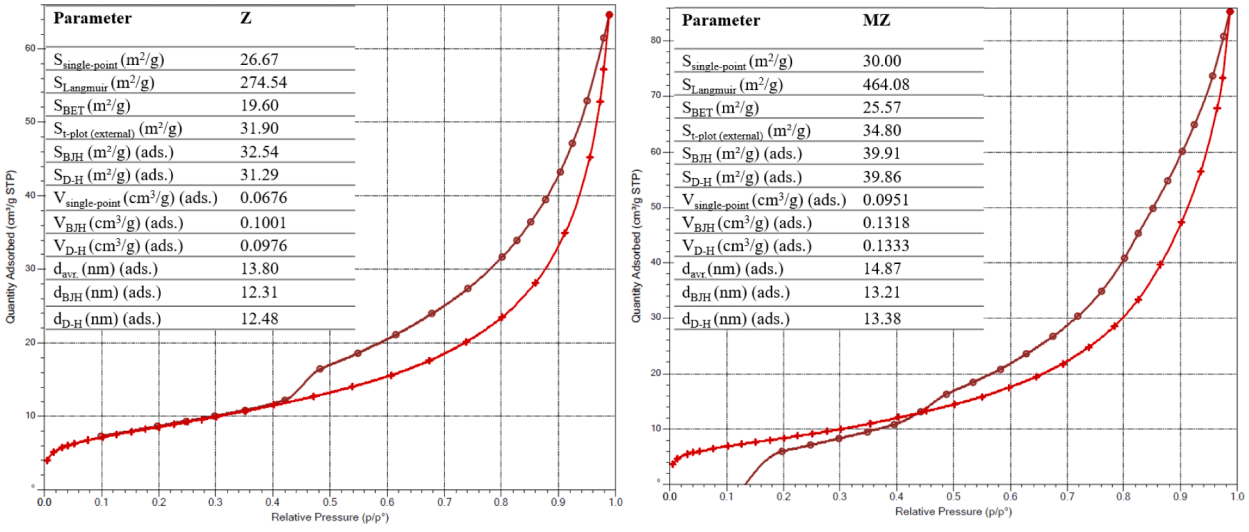

Fig. 2. N_2 adsorption (red) / desorption (claret red) analyses a. Natural zeolite (Z) b. Magnetic zeolite (MZ).

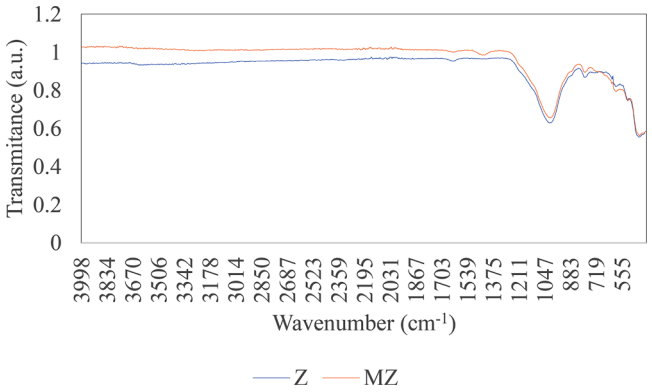

Fig. 4. FTIR analyses of natural zeolite (Z) and magnetic zeolite (MZ).

stability. Therefore, there was no collapse or destruction of the structure by modification of the natural zeolite [36].

3.1.3. FTIR analysis

FTIR analysis provides more information about the structures of the natural and magnetic zeolite due to it reveals the characteristic vibrational bands of the functional groups dominating their structures, as shown in Fig. 4. Clinoptilolite were characterized by bands between 3664 and 3383–2201–2029–1861–1709–852–727–681–571–494 cm^{-1}, respectively [37]. Natural zeolite had its characteristic peaks in the spectral range of 455 cm^{-1} and 1324 cm^{-1} which denotes the T-O-T (T: Al/Si) vibration modes. Also, broad band appearing at 997 cm^{-1} was attributed to the asymmetric stretching vibrations of T-O bonds of TO_4 [21]. A band peaking at ~1647 cm^{-1} associated to bridging O—H groups in Si—OH—Al was observed [38]. Peaks at ~1569–1658 cm^{-1} were attributed to bridging O—H groups that associated with the acidity of natural zeolite. The bands at positions 3623–3383 cm^{-1} indicate the presence of H_2O in natural zeolites [39]. The vibration band occurring at ~636–592–571–494 cm^{-1} represents the internal vibrations due to the asymmetric stretching of Si—O—Al tetrahedral [37]. In Fig. 4, due to the presence of the magnetic particles in the magnetic zeolite, there was a decrease in transmittance (a.u.), but the wavenumber did not change. This situation shows that the internal structure of natural zeolite did not change mainly after magnetic modification [40]. The peak of magnetic zeolite at ~581 cm^{-1} is the characteristic band of Fe—O stretching vibrations of Fe_3O_4 particles. Specific vibrations of Fe—O bonds can be found around 460 cm^{-1} and 570 cm^{-1}. In Fig. 4, it was seen that there were no considerable differences between the natural and magnetic zeolites. But some peaks altered to new values and disappeared. These differences particularly also can be seen in a decrease at the 1526–1321 cm^{-1} band and an increase at 797 cm^{-1}–804 cm^{-1}. These results confirmed the presence of Fe_3O_4 in the magnetic zeolite [41].

3.1.4. SEM-EDX analysis

In Fig. 5a and 5b, cubic and spherical morphology were observed for natural and magnetic zeolites respectively. Spherical morphology of the magnetic zeolite particles was verified by decreasing in crystallinity from XRD results [17]. The presence of voids on the magnetic zeolite surface results from an increase in porosity and surface area as already confirmed from BET results (Fig. 5b) [42]. It was observed that Fe_3O_4 particles clumped together on the zeolite surface and distributed uniformly on the surface due to the interaction of Fe_3O_4 and zeolite. In Fig. 5b, it was seen that the pore voids of the magnetic zeolite increased after the magnetization process [43]. The chemical composition of natural and magnetic zeolites were characterized by EDX analysis. In Fig. 5a, it was found that the main components of natural and magnetic zeolites were Si and Al. Comparison to natural zeolite, the weight rate of Fe in the magnetic zeolite increased from 0.84% to 6.29% which was confirmed from magnetic modification with Fe_3O_4 (Fig. 5b). In Fig. 5, Si/Al ratio were determined as 10.88 and 13.82 for natural and magnetic zeolites respectively. Due to its consisted the high Si/Al ratio,

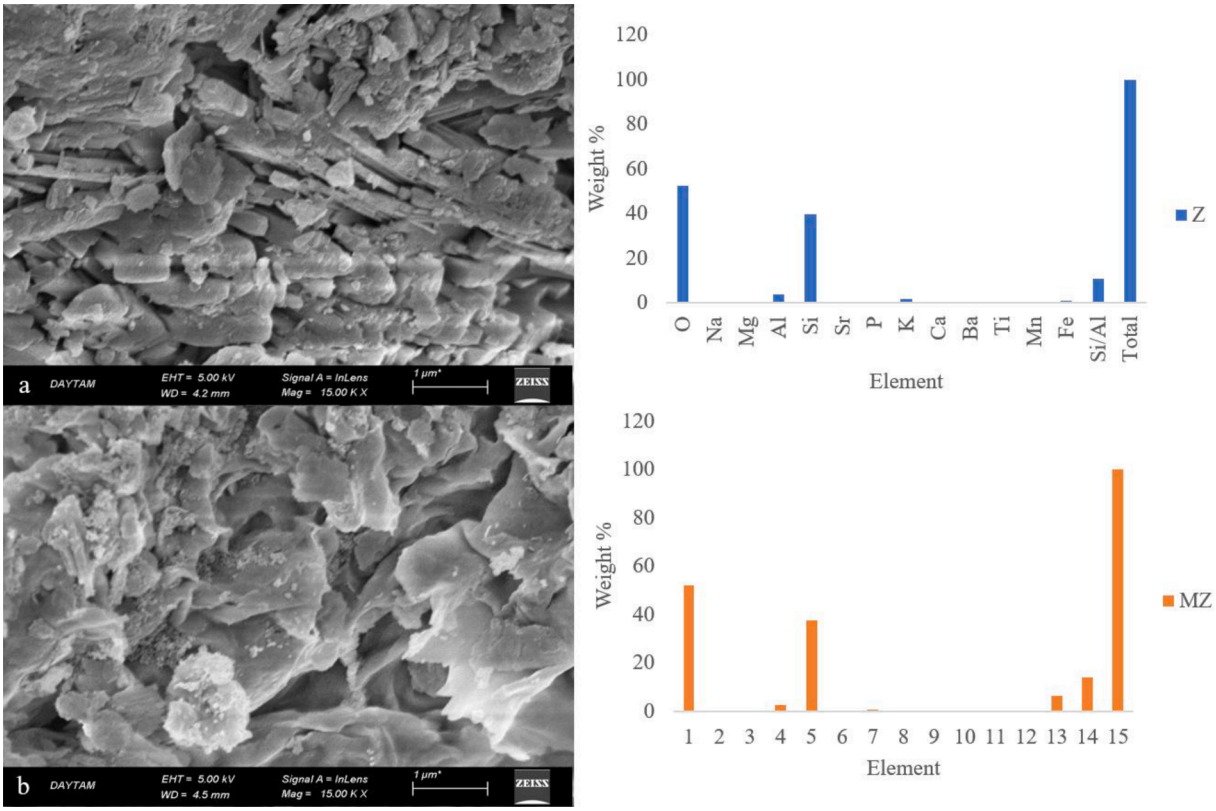

Fig. 5. SEM-EDX analyses a. Natural zeolite (Z) b. Magnetic zeolite (MZ).

magnetic zeolite showed higher adsorption capacity than natural zeolite [44]. It can be seen from Fig. 5a and Fig. 5b that the main exchangeable cations (K^+, Mg^{2+}, Ca^{2+}) exist in the clinoptilolite. Elemental analysis of natural and magnetic zeolites showed that fractions consisted of Si, O, Al, Na, Mg, Ca, K, and Ti [21]. Na^+ were not determined due to experimental error. According to EDX results, big differences in the Si/Al ratio were not determined after magnetic modification [45].

3.1.5. VSM analysis

Magnetic features of magnetic zeolite were analyzed by using a vibrating sample magnetometer in an operational magnetic field from 15 to 15 KO_e at room temperature. As shown in Fig. 6, the adsorbent had a superparamagnetic property that the internal hysteresis loop of the adsorbent showed an "S" shaped curve. The magnetization saturation (M_s) value of magnetic zeolite were determined as 5.421 emu/g for 0.0469 g and 0.25428 emu [46]. The adsorbent had a superparamagnetic property that it does not have any magnetic effect when removing the magnetic field. Superparamagnetic characteristics of zeolite particles can be easily observed using a magnet. When a magnet was placed near the outer wall of a glass tube containing a mixture of zeolite particles and water, these particles were completely absorbed by the magnet [47]. The maximum area (O_e), coercivity (H_{ci}) and permanence (M_r) were determined as 20000 O_e, 11.055 (H_{ci}), and 4.8306E-3 emu respectively. These results confirmed that magnetic zeolite had sufficient magnetic properties that can be attracted by a permanent magnet [34].

3.2. Factors affecting the adsorption of BB41 on natural and magnetic zeolites

3.2.1. Effect of initial pH

Effect of initial pH on BB41 adsorption by natural and magnetic zeolites were examined in the pH range of 4.0–8.0 at 100 mg/L BB41 for 240 min. Experiments were applied with 0–600 μ and 0.1 g natural and magnetic zeolite at 298 K and a constant stirring speed of 200 rpm. The maximum adsorption capacities of BB41 for natural and magnetic zeolites were obtained at pH: 6.0 and pH: 7.0, respectively. It was observed that the adsorption capacities of natural and magnetic zeolites decreased with increasing initial pH above 6.0 and 7.0, respectively (Fig. 7). In general, at a high pH, the percentage of dye removal increases in cationic dye adsorption whereas decreases in anionic dye. At low pH, adsorption is less for cationic dyes due to H^+ ions compete with the cation groups of dye on the adsorption sites. Up to pH: 6.0–7.0, a significantly high electrostatic attraction exists between the negatively charged surface of natural and magnetic zeolites and positively charged of BB41, hence enhancing the dye removal [48]. The maximum adsorption capacities of BB41 for natural and magnetic zeolites were obtained at pH: 6.0 and pH: 7.0, respectively. Adsorption capacity of BB41 by natural zeolite decreased from 72.59 to 67.76 mg/g when pH were increased from 6.0 to 7.0. For magnetic zeolite, it was determined as 73.69 mg/g and 75.78 mg/g at pH: 6.0 and pH: 7.0 respectively. The pH_{pzc} value indicates the type of active sites and the adsorption ability of the adsorbents. When $pH \geq pH_{pzc}$, it is suitable for cationic dye adsorption due to the presence of functional groups such as OH^-, COO^-. The zero charge points of the natural and magnetic zeolites were determined as 6.0 and 7.0 respectively. Natural and magnetic zeolites reacted with BB41 as a negative surface in the range of pH 6.0 and 7.0. It is known that the cationic dye adsorption is more efficient in the case of $pH \geq pH_{pzc}$, while the anionic adsorption increases in the case of $pH \leq pH_{pzc}$. For this reason, the adsorption capacities increased with changing pH values from 4.0 to 6.0–7.0 due to negative charged sites increased. When pH values were higher than 6.0–7.0, the adsorption capacities of natural and magnetic zeolites decreased. Therefore, the adsorption capacities of BB41 were improved by choosing pH values of 6.0 and 7.0 [21,48]. It was reported that Fe_3O_4 has a negatively charged surface at a pH above 5.0. Therefore, the presence of the Fe_3O_4 in magnetic zeolite increased the adsorption capacity by providing new active sites for BB41 adsorption [17].

3.2.2. Effect of adsorbent dosage

The adsorption of BB41 on single natural and magnetic zeolites were studied by changing the quantity of adsorbent dose from 0.025 to 0.2 g at a constant contact time of 240 min. The effect of adsorbent dosage on adsorption were studied at 298 K and 200 rpm with 100 mg/L dye solution and 0–600 μ natural and magnetic zeolites. pH values were adjusted to 6.0 and 7.0 for natural and magnetic zeolites, respectively. In Fig. 7, the adsorption capacities of the BB41 increased up to 0.1 g for natural and magnetic zeolites. The adsorption capacities of the BB41 were determined as 69.40 mg/g and 74.62 mg/g with natural and magnetic zeolites, respectively. This result can be attributed to the increasing in the surface area of natural zeolite with the magnetic modification that was also confirmed from SEM and BET results. The adsorption capacity had a constant value above 0.1 g for each adsorbent. This is because at lower adsorbent dosage, BB41 molecules can easily reach on zeolite surface and dye removal increases per unit of zeolite (Fig. 7) [49].

3.2.3. Effect of particle size

The adsorption of BB41 with natural zeolite were studied by changing the particle size from 0 to 50 μ to 0–600 μ at a constant contact time of 240 min with 100 mg/L dye solution. Experiments were applied with 0.1 g natural and magnetic zeolites at 298 K and a constant stirring speed of 200 rpm. pH values were adjusted to 6.0 and 7.0 for natural and magnetic zeolites, respectively. The highest dye removal was obtained with 0–200 μ particles in natural zeolites and experiments were carried out with 0–200 μ in the magnetic zeolite. It was found that as the particle

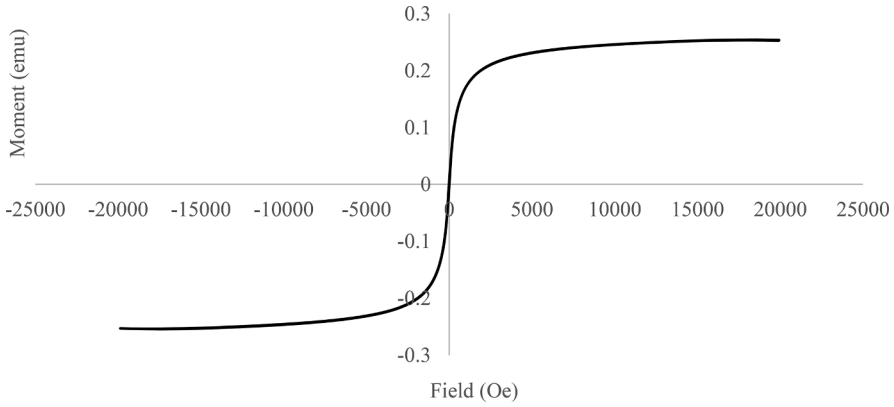

Fig. 6. VSM analysis of magnetic zeolite (m: 0.0469 g, particle size: 0–200 μ).

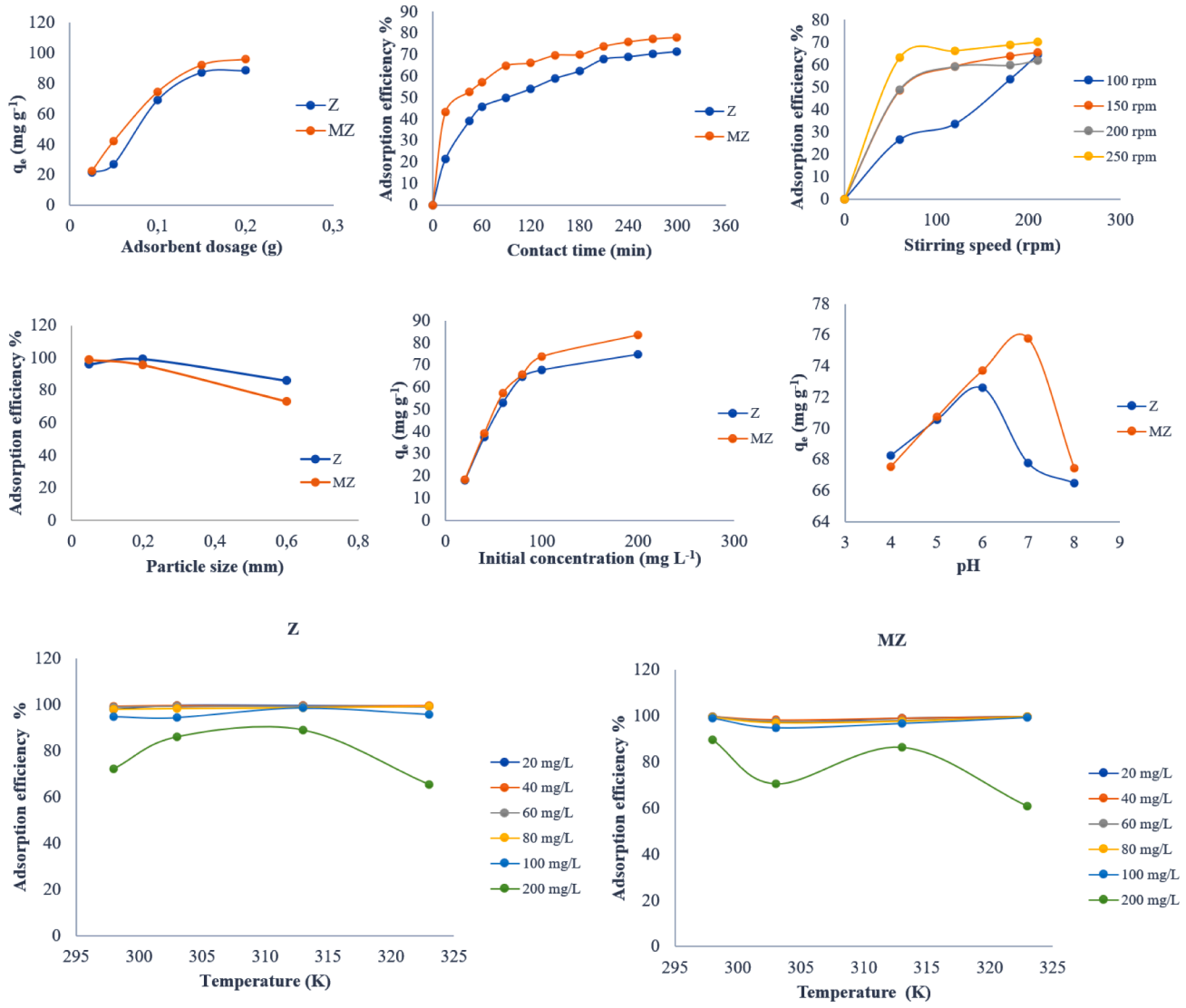

Fig. 7. Factors affecting adsorption of BB41 (Z: Natural zeolite, MZ: Magnetic zeolite).

size increased from 0 to 50 to 0–200 μ, the percentage of dye removal increased from 95.78% to 99.00% (Fig. 7). For magnetic zeolite, the percentage of dye removal were determined as 98.66%, 95.33% and 73.25% in particle sizes of 0–50 μ, 0–200 μ, 0–600 μ, respectively. In general, specific surface area and pore volume increase with a decrease in particle size, and higher adsorption efficiency is obtained. It was observed that dye solution with 0–50 μ particles was like a slurry. In Fig. 7, as the particle size increased to 0–200 μ, the removal efficiency of the natural zeolite increased. But it decreased in magnetic zeolite. This result can be attributed to the decreasing particle size in the natural zeolite due to the strong attractive interaction and agglomeration between the particles and resulting in lower adsorption of dye [50].

3.2.4. *Effect of stirring speed*

The adsorption of BB41 on natural zeolite was studied by changing the stirring speed from 100 rpm to 250 rpm at a constant contact time of 240 min. The effect of stirring speed on adsorption was studied at 298 K and 0.1 g adsorbent with 100 mg/L dye solution and 0–200 μ natural zeolite. pH was adjusted to 6.0. It was observed that dye removal was highest at 250 rpm and experiments were carried out at 250 rpm for magnetic zeolite. It was found that as the stirring rate increased from 100 rpm to 250 rpm the percentage of dye removal increased from 64.44% to 70.03% (Fig. 7). By the higher stirring speed in the BB41-zeolite system, zeolite particles and BB41 molecules started to move faster in the solution and supported the adsorption process. By increasing stirring speed, the transfer resistance from the bulk phase to the zeolite surface decreased at the boundary layer, and the removal percentage of BB41 increased [51].

3.2.5. *Effect of initial concentration*

The effect of BB41 concentration on adsorption were studied at pH: 6.0 and pH: 7.0 with natural and magnetic zeolite, respectively. Experiments were conducted at 240 min, 298 K and a stirring speed of 250 rpm. The adsorbate concentration ranged from 20 to 200 mg/L and 0–200 μ, 0.1 g natural and magnetic zeolites were used. In Fig. 7, it was observed that the adsorption capacities of BB41 on natural and magnetic zeolites increased with increasing initial dye concentration up to 100 mg/L. Adsorption of BB41 reached equilibrium in about 100 mg/L for each adsorbent. The adsorption capacities of the BB41 were determined as 65.79 mg/g and 73.82 mg/g at 100 mg/L with natural and magnetic zeolites, respectively. The results showed that initial dye concentration increased with increasing contact time due to reaching equilibrium. But the amount of adsorbed dye per unit of adsorbent did not change [52]. This is because that the driving force of mass transfer increases with the increasing initial concentration of the dye. In general, dye removal efficiency depends on the relationship between the initial concentration of

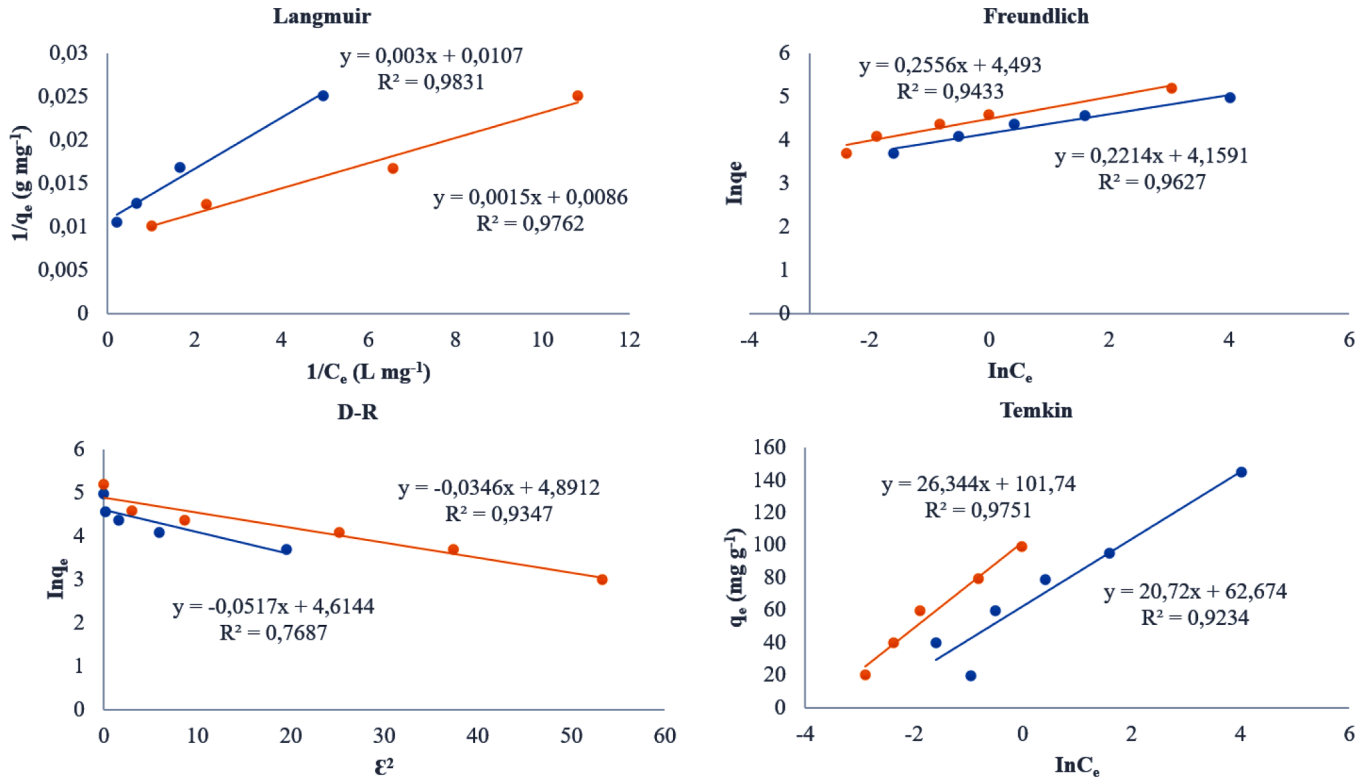

Fig. 8. Linearized Langmuir, Freundlich, Dubinin-Radushkevich (DR) and Temkim isotherms for BB41 adsorption on natural and magnetic zeolites (pH: 6.0 (natural zeolite), pH: 7.0 (magnetic zeolite), T: 298 K, SS: 250 rpm, Co: 20–200 mg/L, particle size: 0–200 μ, adsorbent dosage: 0.1 g).

the solution and adsorption sites on the adsorbent surface. If the adsorption sites on the adsorbent surface are saturated, the percentage removal decreases with increasing initial concentration [53]. If particles (0–200 μ) are rich in natural and magnetic clinoptilolite, adsorption of BB41 might be occurred both by exchangeable cations (K^+, Mg^{2+}, Ca^{2+}) and on the surfaces of the natural and magnetic zeolites due to the presence of the Si-OH groups. The channels and characteristic "cage" structure of the clinoptilolite might result in the diffusion of positive charged BB41 inside the zeolite network. However, average pore sizes of natural and magnetic zeolites were determined as 13.80 nm and 14.87 nm respectively. Considering the sizes of mesopores (d: 2–50 nm) and BB41 cations [21], BB41 can be adsorbed only in certain pores of zeolite structures partially. It can be concluded that adsorption of BB41 mainly occurred on the surface.

3.2.6. *Effect of contact time*

The adsorption of 100 mg/L BB41 with natural and magnetic zeolite were studied by changing contact time from 60 to 240 min at 250 rpm and 298 K. 0–200 μ, 0.1 g adsorbent were used. Experiments were applied with natural and magnetic zeolite at pH 6.0 and 7.0, respectively. In Fig. 7, the adsorption efficiencies% of BB41 increased with increasing contact time until 210 min for natural and magnetic zeolites. The removal efficiency of BB41 reached equilibrium at 210 min then remained constant. It was found that as contact time increased from 60 to 240 min the percentage of dye removal increased from 45.83% to 67.79% for natural zeolite. By magnetic zeolite, an increase was observed from 57.10% to 73.82% within the same period (Fig. 7). This resulted from the presence of more binding sites on the surfaces of the natural and magnetic zeolites at 0–60 min [54]. When contact time increased from 60 to 210 min, there was a significant increase in the amount of dye retained on the same amount of natural and magnetic zeolites. But the amount of adsorbed BB41 molecules remained constant when all sites were occupied on the adsorbent surfaces [55].

3.2.7. *Effect of temperature*

The effect of the temperature on the BB41 adsorption was studied at 250 rpm, 240 min with 0–200 μ, 0.1 g natural and magnetic zeolite. The temperature and initial dye concentration ranged from 298 to 323 K and 20 to 200 mg/L. pH were adjusted to 6.0 and 7.0 for natural and magnetic zeolite, respectively. In Fig. 7, as temperature increased from 298 to 323 K, the percentage of dye removal increased from 95.05% to 95.96% for natural zeolite at 100 mg/L. For magnetic zeolite, an increase was observed from 99.01% to 99.43% within the same temperature and concentration (Fig.7). This result can be attributed to the increasing specific surface area by magnetic modification. For 200 mg/L BB41, adsorption efficiency increased with increasing temperature up to 313 K for only natural zeolite. In Fig. 7, as temperature increased from 313 to 323 K, the percentage of dye removal decreased from 89.12% to 65.62% for natural zeolite at 200 mg/L BB41 concentration. Considering to magnetic zeolite, a decrease was observed from 86.39% to 60.72% within the same temperature at 200 mg/L BB41 concentration. This is because of that decrease of active sites which are suitable for adsorption on surfaces of the natural and magnetic zeolites at high concentrations of BB41 [53].

3.3. *Adsorption isotherms*

In present work, the equilibrium data were analyzed by linear model of Langmuir, Freundlich, Dubinin-Redushkevich (D-R) and Temkin isotherms at 298–323 K (Fig. 8 and Table 1). The results showed that BB41 equilibrium data for natural and magnetic zeolite were well-fitted with the Langmuir model at 298–323 K and calculated correlation coefficients (R^2) for the Langmuir isotherm model have the highest values (Fig. 8 and Table 1). The dimensionless separation factors (R_L) were calculated between $0 < R_L < 1$. Based on dimensionless separation factor, the dye adsorption mechanism was favorable for natural and magnetic zeolites. The dimensionless separation factors (R_L) were determined as between 0.0138–0.0014 and 0.0086–0.0008 with natural

Table 1
Langmuir, Freundlich, Dubinin-Radushkevich (DR) and Temkim isotherm constants for BB41 adsorption on natural and magnetic zeolites (pH: 6.0 (natural zeolite), pH: 7.0 (magnetic zeolite), SS: 250 rpm, Co: 20–200 mg/L, particle size: 0–200 μ, adsorbent dosage: 0.1 g).

	Z			MZ		
T (K)	298	313	323	298	313	323
Langmuir						
q_m (mg/g)	93.45	131.57	149.25	116.27	140.84	370.37
b (L/mg)	3.56	2.92	1.763	5.733	0.73	0.67
R_L	0.0014–0.0138	0.0171–0.0168	0.0028–0.0275	0.0008–0.0086	0.0067–0.0639	0.0073–0.0689
R^2	0.9831	0.9904	0.9836	0.9762	0.9965	0.9998
Feundlich						
N	4.51	2.89	0.86	3.91	2.36	8.10
K_F ((mg/g) (L/mg))$^{1/n}$	64.01	74.23	72.51	89.38	51.32	81.45
R^2	0.9627	0.9125	0.893	0.9433	0.9293	0.8272
D-R						
q_m (mg/g)	100.92	114.74	112.23	133.11	86.33	124.01
k_D (mol^2/kJ^2)	0.0517	0.0331	0.0386	0.0346	0.0753	0.0352
E (kJ/mol)	0.3214	0.257	0.277	0.263	0.388	0.265
R^2	0.7687	0.8962	0.9772	0.9347	0.9672	0.8662
Temkin						
b_T (J/mol)	0.119	0.098	0.207	0.094	0.082	0.071
A (L/g)	20.59	31.03	319.24	47.55	7.39	23.11
R^2	0.9234	0.9859	0.9675	0.9751	0.9882	0.8543

and magnetic zeolites, respectively. It was seen that R_L values decreased with increasing of BB41 concentration from 20 to 200 mg/L. This is because that BB41 adsorption for natural and magnetic zeolites were also favorable at high concentrations. As the R_L values approach zero, adsorption process will lead to irreversible [16]. From the Langmuir Eq. (4), the maximum adsorption capacities of natural and magnetic zeolites were determined as 93.45 and 116.27 mg/g, respectively at 298 K. This result can be attributed to the increasing specific surface area by magnetic modification [56]. BB41 was only adsorbed in a monolayer at the outer interface of the natural and magnetic zeolite [42]. For Langmuir isotherm, the adsorption capacities of natural and magnetic zeolites increased with increasing the temperature and the highest value of adsorption capacity were obtained as 370.37 mg/g at 323 K for magnetic zeolite. The n value in Freundlich isotherm were determined between $1 < n < 10$ for natural and magnetic zeolites at below 323 K. It can be concluded that adsorption was physical and could be suitable for

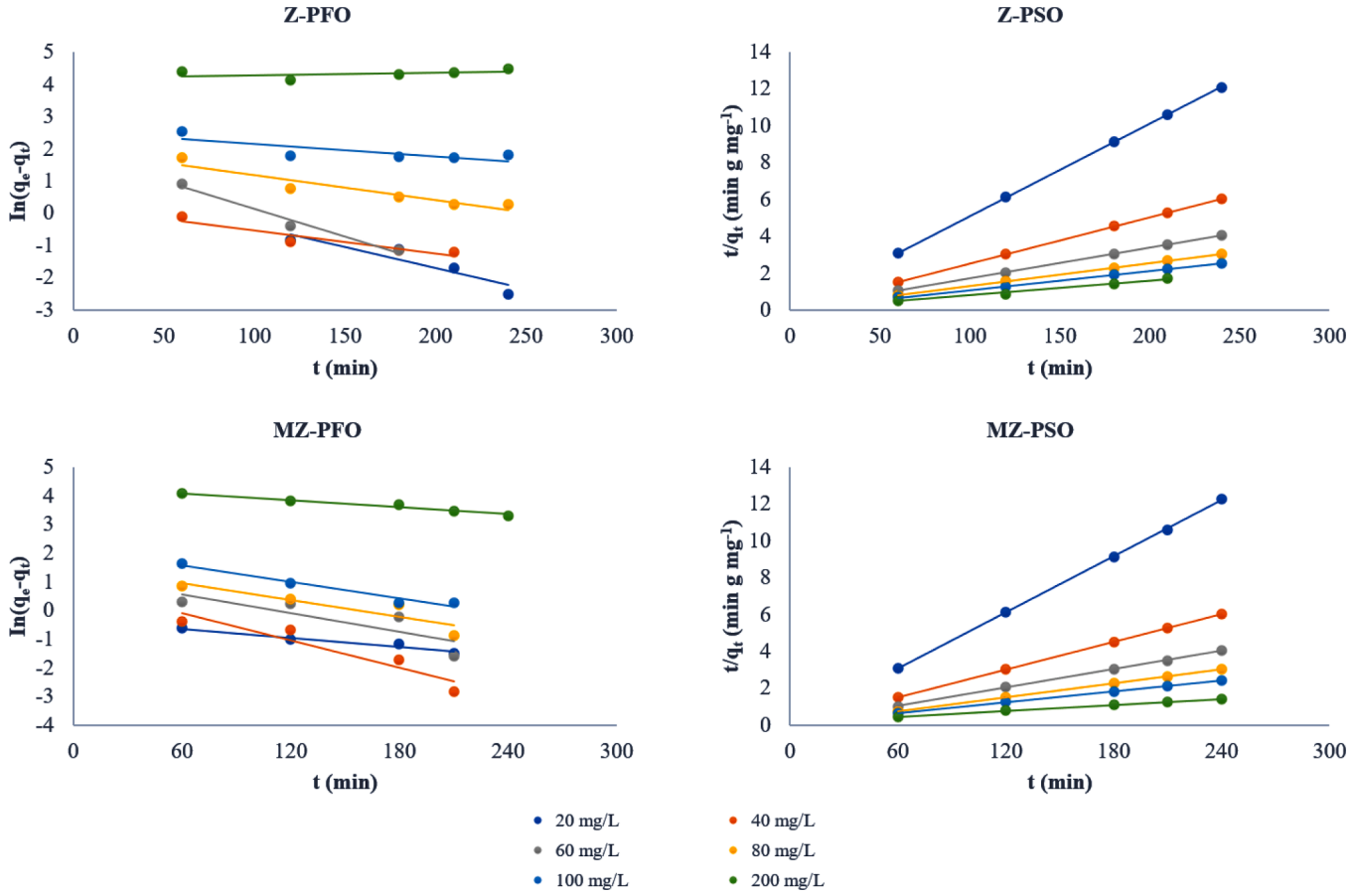

Fig. 9. Pseudo first order (PFO) and pseudo second order (PSO) graphs for BB41 adsorption on natural and magnetic zeolites (pH: 6 (natural zeolite), pH: 7.0 (magnetic zeolite), T: 298 K, SS: 250 rpm, Co: 20–200 mg/L, particle size: 0–200 μ, adsorbent dosage: 0.1 g).

Freundlich isotherm below 323 K [20,57]. The adsorption energies E in the D-R isotherm were less than 8 kJ/mol for both adsorbents and at all temperatures. These results also were confirmed as physical adsorption. The maximum adsorption capacities which were calculated from D-R isotherm models increased up to 313 K for natural zeolite and decreased at 323 K. q_m values of magnetic zeolite were higher than natural zeolite except for 313 K (Table 1). However, the b_T constant in the Temkin model is related to heat absorption and did not show a correlation with the q_m values which was calculated from the Langmuir and D-R isotherms. A decrease or an increase in b_T values were observed between 298 and 323 K for both adsorbents. This can be attributed to the changes in physical interactions such as temperature, Van der Waals, and hydrogen bonds. Furthermore, the Temkin isotherm is more suitable for gas systems [58].

3.4. Adsorption kinetics

The kinetic data for the adsorption of BB41 onto natural and magnetic zeolites were tested with the pseudo first order and pseudo second order models (Fig. 9 and Table 2). The results showed that adsorptions of BB41 on natural and magnetic zeolites did not follow the pseudo first order rate kinetics. From Table 2, it can be clearly seen that the values of the correlation coefficients were not high at the different dye concentrations. Furthermore, the values of q_e calculated from the pseudo first order kinetic model differ significantly from those measured experimentally. The values of q_e calculated from the pseudo second order kinetic model were very close to measured experimental. Correlation coefficients which were calculated from the pseudo second order model were greater than pseudo first order for each adsorbent at 298–323 K. Therefore, BB41 adsorption with natural and magnetic zeolites well described by the pseudo second order model. The k_2 values decreased with increasing the initial dye concentration from 20 mg/L to 200 mg/L, which indicated that the adsorption well described with physical sorption. These results were verified by E (less than 8 kJ/mol) sorption energy values in Dubinin-Radushkevich (D-R) isotherm model [59]. The adsorption process of BB41 with natural zeolite and magnetic zeolites, the mass transfer of BB41 from solution to adsorbent pores can also be considered as the rate control stage [60]. Furthermore, the h (mg/(gmin)) values which were calculated with pseudo second order kinetic constant, k_2, were relatively higher in magnetic zeolite than natural zeolite. This can be attributed to the presence of surface reactions on the magnetic zeolite [61].

3.5. Adsorption thermodynamics

The adsorption mechanism of BB41 on natural and magnetic zeolites were investigated with thermodynamic parameters which include Gibbs free energy change (ΔG), enthalpy change (ΔH) and entropy change (ΔS) at 298–323 K. In the study, ΔG values were determined as negative. It was concluded that adsorption of BB41 onto natural and magnetic zeolites was a spontaneous process. The positive ΔH values indicated that the adsorption was endothermic. The ΔH values were determined as 19.714 kJ/mol and 44.608 kJ/mol for natural and magnetic zeolites, respectively (Table 3). The ΔS values were determined as positive for both adsorbents, and it was higher for magnetic zeolite than natural zeolite. This is because that the increasing randomness at the solid-liquid interface during the adsorption process for magnetic zeolite [23]. Since ΔG values are generally between 20 and 0 kJ/mol for physical sorption, the adsorption mechanism has been realized physically for natural and

Table 3
Thermodynamic parameters calculated from Van't Hoff graph for BB41 adsorption on natural and magnetic zeolites (pH: 6 (natural zeolite), pH: 7.0 (magnetic zeolite), SS: 250 rpm, C_o: 20-200 mg/L, particle size: 0-200 μ, adsorbent dosage: 0.1 g)

Z	T (K)	K_c (L/mg)	ΔG (kJ/mol)	ΔH (kJ/mol)	ΔS (kJ/mol K)
	298	16.303	-13.806	19.714	0.000086
	303	12.825	-14.318		
	313	13.365	-15.117		
	323	23.759	-15.984		
MZ	T (K)	K_c (L/mg)	ΔG (kJ/mol)	ΔH (kJ/mol)	ΔS (kJ/mol K)
	298	18.455	-7.226	44.608	0.000174
	303	40.043	-9.606		
	313	28.556	-8.448		
	323	81.184	-11.812		

Table 2
Kinetic parameters obtained from pseudo first order (PFO) and pseudo second order (PSO) kinetic models for BB41 adsorption on natural and magnetic zeolites (SS: 250 rpm, particle size: 0–200 μ, adsorbent dosage: 0.1 g, exp.: experimental, cal.: calculated).

		PFO				PSO			
T (K)	C_o (mg/L)	q_e (exp.)(mg/g)	q_e (cal.)(mg/g)	k_1 (1/min)	R^2	q_e (cal.) (mg/g)	k_2 (g/(mgmin))	h (mg/(gmin))	R^2
Natural zeolite (Z)									
	20	19.70	2.55	0.0132	0.8528	20.04	0.0226	8.79	0.9999
298	60	59.07	6.29	0.0171	0.9786	60.24	0.0080	27.96	0.9999
	100	92.82	12.55	0.0038	0.6246	96.15	0.0022	19.23	0.9996
	200	123.59	67.85	0.0007	0.1363	99.00	0.0009	15.34	0.9887
	20	19.77	0.86	0.0122	0.9856	19.80	1.1088	433.63	0.9997
313	60	59.83	0.43	0.0072	0.896	59.88	0.0753	269.88	1
	100	92.81	15.42	0.0051	0.8919	98.03	0.0014	12.44	1
	200	127.15	76.54	0.0003	0.0886	129.87	0.0042	69.07	0.9942
	20	19.56	0.98	0.0093	0.9461	19.92	0.0197	7.57	0.9974
323	60	59.57	1.93	0.0092	0.932	59.52	0.1485	527.14	1
	100	94.06	12.08	0.0047	0.9947	98.03	0.0018	16.71	0.9999
	200	120.67	90.44	0.0008	0.3909	126.58	0.0011	17.161	0.9837
Magnetic zeolite (MZ)									
	20	19.62	0.72	0.0053	0.7086	19.68	0.1246	48.03	0.9999
298	60	59.12	3.42	0.0110	0.6738	59.88	0.0122	42.75	0.9998
	100	97.58	8.63	0.0097	0.8304	100	0.0035	33.65	0.9999
	200	129.01	76.58	0.0041	0.8488	135.18	0.0002	6.15	0.9963
	20	19.31	5.61	0.0165	0.9592	20.49	0.0060	2.27	0.9998
313	60	59.30	1.03	0.0037	0.6372	59.52	0.0376	132.36	1
	100	96.52	9.06	0.0068	0.7434	100	0.0024	22.51	0.9998
	200	128.45	5.61	0.0165	0.9592	136.49	0.0060	2.27	0.9998
	20	19.34	1.23	0.0032	0.9829	20.04	0.0104	3.91	0.9989
323	60	59.71	0.43	0.0047	0.9673	59.88	0.0457	163.01	1
	100	98.73	5.11	0.0105	0.9665	55.55	0.0180	175.48	1
	200	112.68	102.73	0.0010	0.7927	125	0.0005	6.67	0.9942

Table 4
Comparison of the adsorption capacities of BB41 on various adsorbents.

Adsorbent	q_m (mg/g)	Ref.
Clinoptilolite/Fe_3O_4 nanocomposite	93.17	[13]
Nanoporous silica	345	[63]
Zeolite A	29	[18]
Zeolite X	88.49	[21]
Local clay mineral from Khulais area	50	[64]
Natural Gördes zeolite	149.25	This work
Magnetic Gördes zeolite	370.37	This work

magnetic zeolites as seen in both PSO kinetic model and D-R isotherm model [20]. When the temperature increased from 298 to 323 K, ΔG values decreased from −13.806 to −15.984 kJ/mol and −7.226 to −11.812 kJ/mol for natural and magnetic zeolites respectively (Table 3). The decrease in values of ΔG with an increase in temperature shows that the ΔH is positive (Eq.18) and ΔG will decrease with increasing temperature. Therefore, adsorption of BB41 on natural and magnetic zeolites was more favorable at higher temperatures [21]. When compared to natural zeolite, the higher enthalpy changes in magnetic zeolite showed that BB41 adsorption on magnetic zeolite can be described with chemical adsorption as well as physical adsorption [62]. As a result, adsoptions of BB41 on natural and magnetic zeolites showed higher adsoption capacities (Table 4) compared to previous studies [13,18,21,63,64].

4. Conclusion

In this study, magnetic zeolite was synthesized from natural Gördes clinoptilolite by chemical co-precipitation method for BB41 adsorption. The characterization results of the natural and magnetic zeolites showed that the magnetization process was successfully achieved, and the greater surface area were obtained from synthesis of magnetic zeolite. VSM analysis showed the presence of ferric particles in the structure of the magnetic zeolite. Comparison to natural zeolite, the intermolecular voids increased, and the crystallinity decreased with magnetic modification. Characteristic peaks of clinoptilolite in zeolite structure were obtained from FTIR analysis. In magnetic zeolite, Fe-O bonds were observed which indicated that Fe_3O_4 loaded in the natural zeolite. XRD analysis showed that the natural and magnetic zeolites were suitable for adsorption of BB41, and that the natural zeolite had structural stability that would not be collapsed after magnetization. Adsorption of BB41 on natural and magnetic zeolites well-fitted by the Langmuir isotherm model and pseudo second order kinetic model. Adsorption was physical, and the weak Van der Waals and electrostatic interactions were effective in the adsorption mechanism. The adsorption processes of natural and magnetic zeolites were found to be spontaneous and endothermic. This study showed that natural and magnetic zeolites can be used efficiently to adsorption of BB41 from textile wastewaters.

Symbols

q_e	Amount of dye adsorbed per gram of adsorbent at equilibrium (mg/g)
q_m	Maximum adsorption capacity (mg/g)
q_t	Dye adsorbed at time t (mg/g)
C_o	Initial dye concentration (mg/L)
C_e	Dye concentration at equilibrium (mg/L)
b	Langmuir isotherm constant (L/g)
R_L	Dimensionless separation factor
K_F	Freundlich isotherm constant ((mg/g)(mg/L)$^{1/n}$)
N	Adsorption intensity
ε	Polanyi potential
k_D	Dubinin-Radushkevich (D-R) isotherm constant (mol^2/kJ^2)
E	Sorption energy (kJ/mol)
A	Equilibrium constant (L/g)
b_T	Temkin isotherm constant (J/mol)
k_1	Pseudo-first-order rate constant (1/min)
k_2	Pseudo-second-order rate constant (g/(mgmin))
h	Initial adsorption rate (mg/(gmin))
R^2	Correlation coefficient
ΔG	Gibbs free energy change (kJ/mol)
ΔH	Enthalpy change (kJ/mol)
ΔS	Entropy change (kJ/mol K)
K_c	Equilibrium constant (L/mg)
t	Time (min)
R	Universal gas constant (kJ/mol K)
T	Temperature (K)
m	Weight of adsorbent (g)
V	Volume of dye solution (L)

Abbreviations

XRD	X-ray diffraction
SEM	Scanning electron microscope
EDX	Energy dispersive X-ray
BET	Brunauer-Emmett-Teller
FTIR	Fourier transform infrared spectroscopy
VSM	Vibrating sample magnetometer
Z	Natural zeolite
MZ	Magnetic zeolite
SS	Stirring speed
PFO	Pseudo first order
PSO	Pseudo second order
Exp.	Experimental
Cal.	Calculated

author agreement

Authors

We confirm that the manuscript has been read and approved by all named authors and that there are no other persons who satisfied the criteria for authorship but are not listed. We further confirm that the order of authors listed in the manuscript has been approved by all of us.

corresponding author

We understand that the Corresponding Author is the sole contact for the Editorial process. She is responsible for communicating with the other authors about progress, submissions of revisions and final approval of proofs.

copyright and plagiarism

We declare that this manuscript is original, has not been published before and is not currently being considered for publication elsewhere.

ethical and legal requirements

We also declare that the study was performed according to the international, national and instutional rules considering animal experiments, clinical studies and biodiversity rights.

financial disclosure

The financial support provided by the Sivas Cumhuriyet University Scientific Research Projects Unit (BAP/M764 coded project) is gratefully acknowledged. The authors gratefully acknowledged zeolite and dye provided by Kuyucak Textile Company-Uşak-Turkey and Gordes Zeolite Company-İzmir-Turkey

Authors' contributions

GM performed the experimental study and was a major contributor in writing the manuscript. ÜA analyzed the experimental data regarding the adsorption studies. ML analyzed the experimental data regarding the adsorption studies. All authors read and approved the final manuscript

Declaration of Competing Interest

The authors declare that they have no known competing financial interests or personal relationships that could have appeared to influence the work reported in this paper.

Supplementary materials

Supplementary material associated with this article can be found, in the online version, at doi:10.1016/j.cep.2021.108632.

References

[1] H. Yuan, L. Chen, Z. Cao, F.F. Hong, Enhanced decolourization efficiency of textile dye Reactive Blue 19 in a horizontal rotating reactor using strips of BNC-immobilized laccase: optimization of conditions and comparison of decolourization efficiency, Biochem. Eng. J. 156 (2020), 107501, https://doi.org/10.1016/j.bej.2020.107501.

[2] S. Popli, U.D. Patel, Destruction of azo dyes by anaerobic–aerobic sequential biological treatment: a review, Int. J. Environ. Sci. Technol. 12 (1) (2014) 405–420, https://doi.org/10.1007/s13762-014-0499-x.

[3] In H. Sadegh, M. Mazloumbilandi, M. Chahardouri, Low-cost materials with adsorption performance (Eds), in: L. Martínez, O. Kharissova, B. Kharisov (Eds.), Handbook of Ecomaterials, Springer, Cham, 2017, https://doi.org/10.1007/978-3-319-48281-1_175-1.

[4] M. Yazdanshenas, K. Farizadeh, A. Fazilat, S. Ahmadi, Adsorption of Basic Blue 41 from aqueous solution onto coconut fiber particles, J. Appl. Chem. Res. 8 (2) (2014) 15–28.

[5] A. Regti, M.R. Laamari, S.E. Stiriba, M.E. Haddad, Removal of Basic Blue 41 dyes using *Persea americana*-activated carbon prepared by phosphoric acid action, Int. J. Ind. Chem. 8 (2017) 187–195, https://doi.org/10.1007/s40090-016-0090-z.

[6] V.K. Gupta, S. Agarwal, A. Olgun, H.İ. Demir, M.L. Yola, N. Atar, Adsorptive properties of molasses modified boron enrichment waste based nanoclay for removal of basic dyes, J. Ind. Eng. Chem. 34 (2016) 244–249, https://doi.org/10.1016/j.jiec.2015.11.017.

[7] S. Afshin, A. Mokhtari, M. Vosoughi, H. Sadeghi, Y. Rashtbari, Data of adsorption of Basic Blue 41 dye from aqueous solutions by activated carbon prepared from filamentous algae, Data Brief 21 (2018) 1008–1013, https://doi.org/10.1016/j.dib.2018.10.023.

[8] M. Mercurio, B. Sarkar, A. Langella, Modified Clay and Zeolite Nanocomposite Materials: Environmental and Pharmaceutical Applications, First Edition, Elsevier, Netherlands, 2019.

[9] M. Sarabadan, H. Bashiri, S. Mousavi, Adsorption of crystal violet dye by a zeolite-montmorillonite nano-adsorbent: modelling, kinetic and equilibrium studies, Clay Miner 54 (4) (2019) 357–368, https://doi.org/10.1180/clm.2019.48.

[10] S. Radoor, Kj. Arayil, J. Parameswaranpillai, S. Siengchin, Removal of anionic dye Congo red from aqueous environment using polyvinyl alcohol/sodium alginate/ZSM-5 zeolite membrane, Sci. Rep. 10 (2020) 15452, https://doi.org/10.1038/s41598-020-72398-5.

[11] M.R. Abukhadra, A.S. Mohamed, Adsorption removal of Safranin dye contaminants from water using various types of natural zeolite, Silicon 11 (2019) 1635–1647, https://doi.org/10.1007/s12633-018-9980-3.

[12] K. Rida, S. Bouraoui, S. Hadnine, Adsorption of methylene blue from aqueous solution by kaolin and zeolite, Appl. Clay Sci. (2013) 99–105, https://doi.org/10.1016/j.clay.2013.08.015, 83-84.

[13] S. Afshin, Y. Rashtbari, M. Vosoughi, R. Rehman, B. Ramavandi, A. Behzad, L. Mitu, Removal of Basic Blue-41 dye from water by stabilized magnetic iron nanoparticles on clinoptilolite zeolite, Rev. Chim. 71 (2) (2020) 218–229, https://doi.org/10.37358/RC.20.2.7919.

[14] A. Badeenezhad, A. Azhdarpoor, S. Bahrami, S. Yousefinejad, Removal of methylene blue dye from aqueous solutions by natural clinoptilolite and clinoptilolite modified by iron oxide nanoparticles, Mol. Simulat. 45 (7) (2019) 564–571, https://doi.org/10.1080/08927022.2018.1564077.

[15] M. Bayat, V. Javanbakht, J. Esmaili, Synthesis of zeolite/nickel ferrite/sodium alginate bionanocomposite via a co-precipitation technique for efficient removal of water-soluble methylene blue dye, Int. J. Biol. Macromol. 116 (2018) 607–619, https://doi.org/10.1016/j.ijbiomac.2018.05.012.

[16] J. Chang, J. Ma, Q. Ma, D. Zhang, N. Qiao, M. Hu, H. Ma, Adsorption of methylene blue onto Fe_3O_4/activated montmorillonite nanocomposite, Appl. Clay Sci. 119 (2016) 132–140, https://doi.org/10.1016/j.clay.2015.06.038.

[17] E. Nyankson, J. Adjasoo, J.K. Efavi, R. Amedalor, A. Yaya, G.P. Manu, K. Asare, N. A. Amartey, Characterization and evaluation of zeolite A/Fe_3O_4 nanocomposite as a potential adsorbent for removal of organic molecules from wastewater, J. Chem. (2019), https://doi.org/10.1155/2019/8090756.

[18] M. Gougazeh, F. Kooli, J.C. Buhl, Removal efficiency of Basic Blue 41 by three zeolites prepared from natural Jordanian kaolin, Clays Clay Miner 67 (2019) 143–153, https://doi.org/10.1007/s42860-019-00016-1.

[19] Y. Aşçi, Ü. Açikel, Y Sağ Açikel, Equilibrium, hysteresis and kinetics of cadmium desorption from sodium-feldspar using rhamnolipid biosurfactant, Environ. Technol. 33 (16) (2012) 1857–1868, https://doi.org/10.1080/09593330.2011.650219.

[20] U.A. Edet, A.O Ifelebuegu, Kinetics, isotherms, and thermodynamic modeling of the adsorption of phosphates from model wastewater using recycled brick waste, Processes 8 (6) (2020) 665, https://doi.org/10.3390/pr8060665.

[21] I. Humelnicu, A. Băiceanu, M.E. Ignat, V. Dulman, The removal of Basic Blue 41 textile dye from aqueous solution by adsorption onto natural zeolitic tuff: kinetics and thermodynamics, Process Saf. Environ. Prot. 105 (2017) 274–287, https://doi.org/10.1016/j.psep.2016.11.016.

[22] E.A. Alabbad, Efficacy assessment of natural zeolite containing wastewater on the adsorption behaviour of Direct Yellow 50 from; equilibrium, kinetics and thermodynamic studies, Arab. J. Chem. 14 (4) (2021), 103041, https://doi.org/10.1016/j.arabjc.2021.103041.

[23] W. Huang, J. Chen, F. He, J. Tang, D. Li, Y. Zhu, Y. Zhang, Effective phosphate adsorption by Zr/Al-pillared montmorillonite: insight into equilibrium, kinetics and thermodynamics, Appl. Clay Sci. 104 (2015) 252–260, https://doi.org/10.1016/j.clay.2014.12.002.

[24] L.C.A. Oliveira, D.I. Petkowicz, A. Smaniotto, S.B.C. Pergher, Magnetic zeolites: a new adsorbent for removal of metallic contaminants from water, Water Res. 38 (17) (2004) 3699–3704, https://doi.org/10.1016/j.watres.2004.06.008.

[25] Z. Majid, A.A. Abdulrazak, W.A.H. Noori, Modification of zeolite by magnetic nanoparticles for organic dye removal, Arab. J. Sci. Eng. 44 (2019) 5457–5474, https://doi.org/10.1007/s13369-019-03788-9.

[26] R. Foroutan, R. Mohammadi, J. Razeghi, B. Ramavandi, Performance of algal activated carbon/Fe_3O_4 magnetic composite for cationic dyes removal from aqueous solutions, Algal. Res. 40 (2019), 101509, https://doi.org/10.1016/j.algal.2019.101509.

[27] M. Thommes, K. Kaneko, A.V. Neimark, J.P. Olivier, F. Rodriguez-Reinoso, J. Rouquerol, K.S.W. Sing, Physisorption of gases, with special reference to the evaluation of surface area and pore size distribution (IUPAC Technical Report), Pure Appl. Chem. 87 (9–10) (2015), https://doi.org/10.1515/pac-2014-1117.

[28] A. Sachse, A. Grau-Atienza, E.O. Jardim, N. Linares, M. Thommes, J. García-Martínez, Development of intracrystalline mesoporosity in zeolites through surfactant-templating, Cryst. Growth Des. 17 (2017) 4289–4305, https://doi.org/10.1021/acs.cgd.7b00619.

[29] S.S. Yudha, M. Adfa, A. Falahudin, Eco-friendly coating of natural zeolite with metallic gold, and characterization of the resulting products, Orient. J. Chem. 34 (1) (2018) 532–537, https://doi.org/10.13005/ojc/340160.

[30] M. Dosa, M. Piumetti, S. Bensaid, N. Russo, O. Baglieri, F. Miglietta, D. Fino, Properties of the clinoptilolite: characterization and adsorption tests with methylene blue, J. Adv. Catal. Sci. Techno. 5 (2018) 1–10, https://doi.org/10.15379/2408-9834.2018.05.01.01.

[31] E.Ö. Tufan, Ion Exchange Properties of Gördes clinoptilolite: Ammonium exchange, Msc. Thesis, Metu, Ankara, 2002.

[32] R. Szostak, Handbook of Molecular Sieves, Van Nostrand Reinhold, New York, 1984.

[33] F. Rahmani, M. Haghighi, M. Amini, The beneficial utilization of natural zeolite in preparation of Cr/clinoptilolite nanocatalyst used in CO_2-oxidative dehydrogenation of ethane to ethylene, J. Ind. Eng. Chem. 31 (2015) 142–155, https://doi.org/10.1016/j.jiec.2015.06.018.

[34] O. Falyouna, O. Eljamal, I. Maamoun, A. Tahara, Y. Sugihara, Magnetic zeolite synthesis for efficient removal of cesium in a lab-scale continuous treatment system, J. Colloid Interface Sci. 571 (2020) 66–79, https://doi.org/10.1016/j.jcis.2020.03.028.

[35] Y. Abdellaouia, M.T. Olguinb, M. Abatalc, A. Bassama, G. Giácoman-Vallejo, Relationship between Si/Al ratio and the sorption of Cd(II) by natural and modified clinoptilolite-rich tuff with sulfuric acid, Desal. Water Treat. 150 (2019) 157–165, https://doi.org/10.5004/dwt.2019.23792.

[36] A. Rivera, T. Farías, L.C. De Ménorval, G. Autié-Castro, H. Yee-Madeira, J. L. Contreras, M. Autié-Pérez, Acid natural clinoptilolite: structural properties against adsorption/separation of n-paraffins, J. Colloid Interface Sci. 360 (1) (2011) 220–226, https://doi.org/10.1016/j.jcis.2011.04.035.

[37] A. Mohseni-Bandpi, T.J. Al-Musawi, E. Ghahramani, M. Zarrabi, S. Mohebi, S. A. Vahed, Improvement of zeolite adsorption capacity for Cephalexin by coating with magnetic Fe_3O_4 nanoparticles, J. Mol. Liq. 218 (2016) 615–624, https://doi.org/10.1016/j.molliq.2016.02.092.

[38] R. Nosrati, A. Olad, K. Nofouzi, A self-cleaning coating based on commercial grade polyacrylic latex modified by TiO_2/Ag-exchanged-zeolite-A nanocomposite, Appl. Surf. Sci. 346 (2015) 543–553, https://doi.org/10.1016/j.apsusc.2015.04.056.

[39] K. Chakarova, K. Hadjiivanov, FTIR study of N_2 and CO adsorption on H-D-FER, Micropor. Mesopor. Mat. 177 (2013) 59–65, https://doi.org/10.1016/j.micromeso.2013.04.022.

[40] M.R. Samarghandi, T.J. Al-Musawi, A. Mohseni-Bandpi, M. Zarrabi, Adsorption of Cephalexin from aqueous solution using natural zeolite and zeolite coated with manganese oxide nanoparticles, J. Mol. Liq. 211 (2015) 431–441, https://doi.org/10.1016/j.molliq.2015.06.067.

[41] J. Cao, Q. Sun, P. Wang, J. Shen, X. Dai, Synthesize and characterize of Fe_3O_4/Zeolite 4A magnetic nanocomposite, J. Disper. Sci. Technol. (2020), https://doi.org/10.1080/01932691.2020.1843480.

[42] F.S. Hashem, Adsorption of methylene blue from aqueous solutions using Fe_3O_4/bentonite nanocomposite, Hydrol. Current Res. 3 (143) (2012), https://doi.org/10.4172/2157-7587.1000143.

[43] A. Hamedi, F. Trotta, M. Borhani Zarandi, M. Zanetti, F. Caldera, A. Anceschi, M. R. Nateghi, In situ synthesis of MIL-100(Fe) at the surface of Fe_3O_4@AC as highly efficient dye adsorbing nanocomposite, Int. J. Mol. Sci. 20 (22) (2019) 5612, https://doi.org/10.3390/ijms20225612.

[44] H.F. Chen, Y.J. Lin, B.H. Chen, I. Yoshiyuki, S. Liou, R.T. Huang, A further investigation of NH_4^+ removal mechanisms by using natural and synthetic zeolites

in different concentrations and temperatures, Minerals 8 (11) (2018) 499, https://doi.org/10.3390/min8110499.
[45] H. Ramezani, S.N. Azizi, G. Cravotto, Improved removal of methylene blue on modified hierarchical zeolite Y: achieved by a "destructive-constructive" method, Green Process Synth. 8 (1) (2019) 730–741, https://doi.org/10.1515/gps-2019-0043.
[46] V. Javanbakht, S.M. Ghoreishi, N. Habibi, Et Al, Synthesis of zeolite/magnetite nanocomposite and a fast experimental determination of its specific surface area, Prot. Met. Phys. Chem. Surf. 5 (2017) 693–702, https://doi.org/10.1134/S2070205117040086.
[47] Y. Chen, K. Liu, Magnetic Ce-doped TiO_2/$NiFe_2O_4$/diatomite ternary composite: enhanced visible-light-driven photocatalytic performance, Powder Technol. 313 (2017) 44–53, https://doi.org/10.1016/j.powtec.2017.03.005.
[48] P. Qin, Y. Yang, X. Zhang, J. Niu, H. Yang, S. Tian, J. Zhu, M. Lu, Highly efficient, rapid, and simultaneous removal of cationic dyes from aqueous solution using monodispersed mesoporous silica nanoparticles as the adsorbent, Nanomaterials 8 (1) (2017) 4, https://doi.org/10.3390/nano8010004.
[49] M.K. Sachin, R.W. Gaikwad, Removal of methylene blue from effluent by using activated carbon and water hyacinth as adsorbent, Int. J. Chem. Eng. Appl. 2 (5) (2011) 317–319, https://doi.org/10.7763/IJCEA.2011.V2.126.
[50] Y. Huang, K. Wang, D. Dong, D. Li, M.R. Hill, A.J. Hill, H. Wang, Synthesis of hierarchical porous zeolite NaY particles with controllable particle sizes, Micropor. Mesopor. Mat. 127 (3) (2010) 167–175, https://doi.org/10.1016/j.micromeso.2009.07.026.
[51] C.E.De F. Silva, B.M.V.Da Gama, A.H.Da S. Gonçalves, J.A. Medeiros, A.K. De S Abud, Basic-dye adsorption in albedo residue: effect of pH, contact time, temperature, dye concentration, biomass dosage, rotation and ionic strength, J. King Saud Univ. Eng. Sci. 32 (6) (2019) 351–359, https://doi.org/10.1016/j.jksues.2019.04.006.
[52] A.N. Alene, G.Y. Abate, A.T. Habte, Bioadsorption of Basic Blue dye from aqueous solution onto raw and modified waste ash as economical alternative bioadsorbent, J. Chem. (2020) 1–11, https://doi.org/10.1155/2020/8746035.
[53] B. Baheri, R. Ghahremani, M. Peydayesh, M. Shahverdi, T. Mohammadi, Dye removal using 4A-zeolite/polyvinyl alcohol mixed matrix membrane adsorbents: preparation, characterization, adsorption, kinetics, and thermodynamics, Res. Chem. Intermed. 42 (6) (2015) 5309–5328, https://doi.org/10.1007/s11164-015-2362-1.
[54] M.V. Niri, A.H. Mahvi, M. Alimohammadi, M. Shirmardi, H. Golastanifar, M. J. Mohammadi, A. Naeimabadi, M. Khishdost, Removal of natural organic matter (NOM) from an aqueous solution by NaCl and surfactant-modified clinoptilolite, J. Water Health. 13 (2) (2015) 394–405, https://doi.org/10.2166/wh.2014.088.
[55] H. Bendjeffal, M. Ziati, A. Aloui, H. Mamine, T. Metidji, A. Djebli, Y. Bouhedja, Adsorption and removal of hydroxychloroquine from aqueous media using Algerian kaolin: full factorial optimisation, kinetic, thermodynamic, and equilibrium studies, Int. J. Environ. Anal. Chem. (2021), https://doi.org/10.1080/03067319.2021.1887162.
[56] S. Nethaji, A. Sivasamy, A.B. Mandal, Adsorption isotherms, kinetics and mechanism for the adsorption of cationic and anionic dyes onto carbonaceous particles prepared from Juglans regia shell biomass, Int. J. Environ. Sci. Technol. 10 (2013) 231–242, https://doi.org/10.1007/s13762-012-0112-0.
[57] E. Ajenifuja, J.A. Ajao, E.O.B. Ajayi, Adsorption isotherm studies of Cu(II) and Co (II) in high concentration aqueous solutions on photocatalytically modified diatomaceous ceramic adsorbents, Appl. Water Sci. 7 (7) (2017) 3793–3801, https://doi.org/10.1007/s13201-017-0527-3.
[58] M. Amin, A. Alazba, M. Shafiq, Adsorptive removal of Reactive Black 5 from wastewater using bentonite clay: isotherms, kinetics and thermodynamics, Sustainability 7 (11) (2015) 15302–15318, https://doi.org/10.3390/su71115302.
[59] W.M. Algothmi, N.M. Bandaru, Y. Yu, J.G. Shapter, A.V. Ellis, Alginate-graphene oxide hybrid gel beads: an efficient copper adsorbent material, J. Colloid Interface Sci. 397 (2013) 32–38, https://doi.org/10.1016/j.jcis.2013.01.051.
[60] N. Mosallanejad, A. Arami, Kinetics and isotherm of Sunset Yellow dye adsorption on cadmium sulfide nanoparticle loaded on activated carbon, J. Chem. Health Risks 2 (1) (2012) 31–40, https://doi.org/10.22034/JCHR.2012.543986.
[61] C.T. Wang, W.L. Chou, M.H. Chung, Y.M. Kuo, COD removal from real dyeing wastewater by electro-Fenton technology using an activated carbon fiber cathode, Desalination 253 (1–3) (2010) 129–134, https://doi.org/10.1016/j.desal.2009.11.020.
[62] H. Mittal, R. Babu, A.A. Dabbawala, S.M. Alhassan, Low-temperature synthesis of magnetic carbonaceous materials coated with nanosilica for rapid adsorption of methylene blue, ACS Omega 5 (11) (2020) 6100–6112, https://doi.org/10.1021/acsomega.0c00093.
[63] M. Zarezadeh-Mehrizi, A. Badiei, Highly efficient removal of Basic Blue 41 with nanoporous silica, Water Resour. Ind. 5 (2014) 49–57, https://doi.org/10.1016/j.wri.2014.04.002.
[64] F. Kooli, Y. Liu, R. Al-Faze, A. Al Suhaimi, Effect of acid activation of Saudi local clay mineral on removal properties of Basic Blue 41 from an aqueous solution, Appl. Clay Sci. (2015) 23–30, https://doi.org/10.1016/j.clay.2015.07.044, 116-117.